ACCSCIENCE PUBLISHING

Design+

ARTICLE

Closed-form solution for pressurized obround shells

Yao Jin*

Propak Systems Ltd., Airdrie, Alberta, Canada

Abstract

Pressurized shells with an obround cross-section are common components in the petrochemical industry. However, the analysis and design of obround components have been challenging due to their complex shapes. Empirical and numerical methods are commonly used for their analysis and design. In this study, the obround shape is divided into curved and straight segments to simplify the geometry and boundary conditions within each segment. The theoretical analysis of each segment was performed separately. By combining existing closed-form solutions, a theoretical solution was developed that partially satisfies the deformation at the junction of segments. This combined solution can accurately calculate stress and displacement in obround shells under internal pressure, representing a closed-form theoretical solution for pressurized obround shells. When the length of the straight segments approaches zero, the obround shell becomes cylinder, the proposed solution returns to the solution of cylindrical shell or Lame's solution. The solution provides a new theoretical analysis approach that is simpler, more efficient, and more accurate than empirical methods or numerical analyses. It is expected to change the current reliance on empirical formulas and numerical simulations for analyzing obround components and to promote the development of a new design methodology for obround components.

Keywords: Obround; Pressure vessel; Non-circular; Stress analysis; Theoretical analysis; Closed-form solution

***Corresponding author:**
Yao Jin
(mtjinyao1@hotmail.com)

Citation: Jin Y. Closed-form solution for pressurized obround shells. *Design+* 2025;2(2):025060010. doi: 10.36922/DP025060010

Received: February 8, 2025

Revised: March 13, 2025

Accepted: April 17, 2025

Published online: April 30, 2025

1. Introduction

Spheres and cylinders are optimal shapes for internal pressure vessels due to their circular cross-sections, which allow for smooth and relatively uniform stress and displacement distributions under internal pressure. However, in certain applications, these shapes are not suitable, and an obround cross-section may be a more appropriate option.

Theoretical analysis of obround shapes is challenging due to their complex and discontinuous geometry. At present, no theoretical solution exists. The analysis and design of obround components rely on empirical and/or numerical methods. Designing an obround enclosure often involves a complex iterative design process.[1,2]

One of the most commonly used empirical methods for analyzing and designing members with non-circular cross-sections is based on the concept of an "equivalent circular section," introduced by Blach.[3] In this method, a non-circular cross-section is

simplified to an equivalent circular one. This allows the use of a circular member design process for non-circular members.

The American Society of Mechanical Engineers (s) code adopted this concept by proposing a design-by-role method. In this approach, stresses at three potentially high-stress locations are estimated using empirical formulas and pre-estimated shell thicknesses. The maximum stress obtained needs to be compared with the allowable stress to confirm whether the pre-estimated thickness is acceptable. If the estimated thickness is found to be inappropriate, adjustments must be done. The maximum stresses are then recalculated and compared until an acceptable thickness is obtained.[1,2]

Even if the shell thickness is deemed acceptable, the true stress within the shell remains unknown due to the inaccuracy of empirical formulas. As a result, the thickness obtained through this process is not necessarily the minimum required. While this approach is generally safe, it may become overly conservative as the length-to-width ratio of the obround increases.[3]

At present, there is no empirical formula in design codes for estimating the displacement of obround shells. The deformation of obround components is typically determined using numerical analysis methods.

Zheng[4] carried out a theoretical analysis of non-circular cross-sections. The explicit form of the elastic governing equations for non-circular cross-section shell geometries was developed using general shell equations, the energy method, and various integral formulations. For an elliptical shell whose geometry is relatively simple and can be described by a continuous function, expressions of shell forces, shear forces, and bending moments were derived under internal pressure and body forces.

Singh[5] performed a theoretical analysis of obround shells with reinforced gussets. A design method was proposed to determine the appropriate gusset plate locations to reinforce the pressurized obround shells.

To improve the accuracy of analysis and design, finite element analysis (FEA) is increasingly employed for non-circular pressure vessels. Shah and Pradhan[6] used FEA for stress analysis of an obround flange. Utagikar and Naik[7,8] analyzed the stress and deformation in obround and elliptical pressure vessels. Pany[9] conducted a non-linear FEA to study the stress states in open-ended pressure vessels with various cross-sections (circular, elliptical, and obround).

In the present study, the theory of elasticity is used to derive a closed-form solution for obround shells. According to this approach, the solution to a two-dimensional or axisymmetric problem is to find a stress function that satisfies the boundary conditions.[10]

As an obround shape consists of straight and circular sections, finding a stress function that satisfies both straight and circular boundaries is extremely difficult, if not impossible. Therefore, it is more practical to use separate stress functions to satisfy different boundary conditions.

In this study, the obround shape is divided into curved and straight segments, each with relatively simple geometry and load boundary conditions.

For a straight or circular segment with simple boundary loads, theoretical solutions are available. By using the superposition principle, introducing reasonable assumptions, and combining existing closed-form solutions of elastic theory, a closed-form solution for obround components under internal pressure is developed. This solution can be used to calculate stresses and displacements at locations of interest.

Considering the uniqueness of the elastic solution, this formulation represents the closed-form theoretical solution for pressurized obround shells.

Because the stresses calculated using the proposed method are accurate, it is possible to determine the minimum required thickness.[12] In addition, this method can be applied to out-of-roundness analysis.[13]

2. Theoretic analysis

Figure 1 shows the obround shape or cross-section of the shell, which consists of curved and straight segments. In this study, the length of the shell is limited to unit length, and the analytical model is limited to a plane stress state. However, the results should be applicable to both plane stress and plane strain states. The term "section" refers to a section through the wall thickness and perpendicular to the thickness, that is, sections A, B, C, and D in Figure 1. The origin of the global rectangular coordinates is placed at the section center.

Letters *a* and *b* represent the inside and outside radius of the curved segment or half of the inside and outside

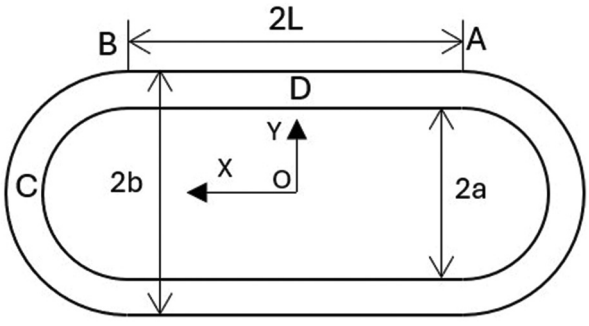

Figure 1. Obround cross-section

dimensions. The wall thickness, *b-a*, is uniform along the cross-section. *L* denotes the half-length of the straight segment, and pressure *p* is applied to the inner surface.

Sections A and B mark the junctions between the curved and straight segments. Sections C and D lie on the planes of symmetry, that is, Y=0 and X=0, respectively.

Considering the symmetry conditions, the analysis model selected is shown in Figure 2. All internal forces and moments at sections A and C were treated as external loads, which acted as load boundaries.

As section C lies along a plane of symmetry, no shear force exists in this section. The total number of unknown loads to be determined at the boundaries was five (Figure 2).

Because the forces and bending moments act over unit lengths, their units are N/m and N-m/m, respectively.

Based on force equilibrium conditions, four equations can be formulated among the five unknown loads.

$$F_x=pa \quad (I)$$

$$F_y=p(a+L) \quad (II)$$

$$F_{Ay}=PL \quad (III)$$

$$M_C=M_A-pL(a+b)/2 \quad (IV)$$

The load directions are shown in Figure 2.

Three forces can be calculated using Equations I – III. However, only one equation relates the two bending moments M_A and M_C so an additional expression is needed to solve the equations.

To introduce this additional expression, the analysis object was divided into two parts: A curved segment BC, which represents a quarter of a ring, and a straight segment AB (Figure 3).

Due to the symmetry condition, there is no section rotation or shear force at section C. The horizontal displacement at the center of this section can be considered rigid body motion and thus ignored. The segment can be thought of as a curved beam with one end fixed and the other free to move. The load conditions included forces and moments acting at the free end, as well as pressure acting on the inner surface (left of Figure 3).

The straight segment AB can be treated as a simple support beam, with a potential rigid body motion v_0 in the vertical direction at the supports, which is induced by the curved segment. Due to the symmetric condition, the load values at both ends of the beam are identical, i.e., $F_{By}=F_{Ay}$, $M_B=M_A$ (right of Figure 3).

Section B is the common section or junction between the curved segment BC and the straight segment AB. All mechanical variables in this section, such as stress, strain, and displacement, should ideally be continuous at section B.

However, as section B is defined as a load boundary rather than a displacement boundary, it is impossible to ensure the complete continuity of all variables. As an approximation, only the displacement and rotation angle at the section center are required to be continuous.

In this study, the rotation angle of a section is defined as the rotation angle of a small element located at the center of the section and along thickness. Clockwise rotation is considered the positive rotation angle (Figure 4).

2.1. Rotation angle of section B

2.1.1. Curved segment BC

A local polar coordinate system is adopted in the analysis. The local coordinate origin is located at the center of the curved beam BC, with θ measured from section C.

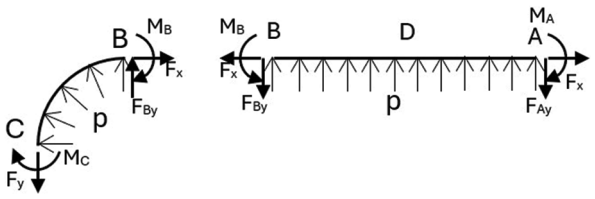

Figure 3. Loads on segment ends

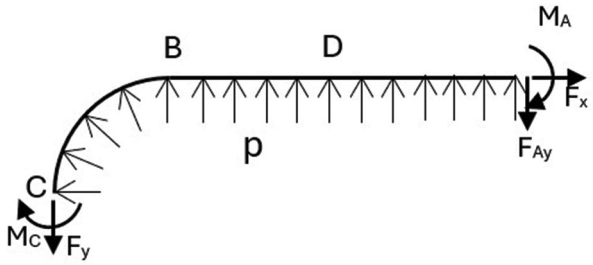

Figure 2. Analysis object

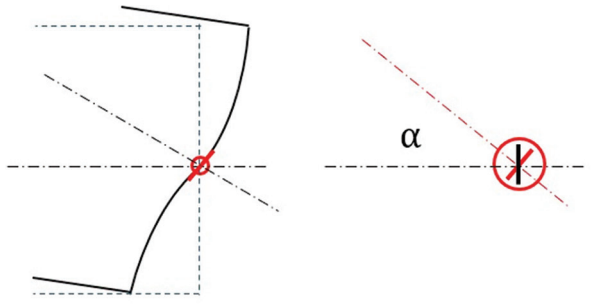

Figure 4. Section rotation

That is, the coordinates of the center of section C are $r = r_0 = \frac{a+b}{2}$, $\theta = 0$ or $X = L + \frac{a+b}{2}$, $Y = 0$ for global coordinates.

In the analysis (except for the pressure load), section C was assumed to be fixed, and section B is free to move. The load boundary conditions consisted of a superposition of the inner surface pressure *p*, free end bending moment M_B, tangential force F_x, and radial force F_{By}. In the local polar coordinates, the section rotation angle is defined as $(\partial v_t / \partial r)_{r=r_0}$, where v_t and r are the tangential displacement component and radial coordinate, respectively.

2.1.1.1. Internal pressure, p

Segment BC is a quarter ring, with section C serving as the plane of symmetry. Under internal pressure *p*, if section B is also a plane of symmetry, the issue becomes axisymmetric. In that case, the closed-form solution is available.[10,11]

In an axisymmetric issue or a pressurized ring, the tangential stress σ_θ, bending moment M_{B1}, and tangential force F_x are identical across any section.

$$\sigma_\theta = \frac{pa^2}{b^2 - a^2}\left(\frac{b^2}{r^2} + 1\right) \quad \text{(V)}$$

$$M_{B1} = \int_a^b \sigma_\theta (r - r_0)\,dr = p\left(\frac{a^2 b^2}{b^2 - a^2}\ln\frac{b}{a} - \frac{ab}{2}\right) \quad \text{(VI)}$$

$$F_x = \int_a^b \sigma_\theta\,dr = pa \quad \text{(VII)}$$

To maintain the state of a pressurized ring, the tangential stress distribution at section B must be the same as that described in Equation V. However, if it is not the same but the loads are equivalent to those of Equations VI and VII, the stress distribution of Equation V is still valid beyond section B, according to Saint-Venant's principle.

The tangential force F_x obtained from Lame's solution, Equation VII also agrees with that obtained from force equilibrium (Equation I). As this force is necessary to maintain the pressurized ring state, it does not need to be considered when calculating the section rotation.

As this is an axisymmetric solution, the internal pressure does not induce any rotation of the section.

2.1.1.2. Bending moment, M_{B2}

As the bending moment M_{B1} is required to maintain the pressurized ring state, the bending moment to be considered should be $M_{B2} = M_B - M_{B1}$.

When section C is fixed and a bending moment M_{B2} is applied to the free end (section B), the rotation angle of section B is given by Timoshenko & Goodier,[10] Xu[11]:

$$\alpha_1 = \frac{4\pi\left(b^2 - a^2\right)}{N_1 E} M_{B2} \quad \text{(VIII)}$$

where:

$$N_1 = (b^2 - a^2)^2 - 4a^2 b^2 \left(\ln\frac{b}{a}\right)^2 \quad \text{(IX)}$$

$$M_{B2} = M_B + \frac{1}{2}pab - \frac{pa^2 b^2}{b^2 - a^2}\ln\left(\frac{b}{a}\right) \quad \text{(X)}$$

Here, E is Young's modulus of the material.

2.1.1.3. Radial force, pL

If the bending moment described in Section 2.1.1.2 is replaced by the radial force F_{By}=pL, as shown on the left side of Figure 3, the rotation angle of section B can be calculated using Equation XI:[10,11]

$$\alpha_2 = -p\,K_1/E \quad \text{(XI)}$$

where:

$$K_1 = \frac{L}{N_2}\left[(5+\mu)r_0 + (1+\mu)\frac{a^2 b^2}{r_0^3} + (1-\mu)\frac{b^2 + a^2}{r_0}\right] \quad \text{(XII)}$$

$$N_2 = \left(b^2 + a^2\right)\ln\frac{b}{a} - \left(b^2 - a^2\right) \quad \text{(XIII)}$$

Here, μ is the Poisson's ratio of the material.

2.1.2. Straight segment AB

A local rectangular coordinate system is adopted in the straight segment analysis. The origin of the coordinates is located at the center of section D. The directions of x and y are the same as those of global X and Y.

The straight segment AB can be regarded as a simple supported beam with uniformly distributed load *p*, a bending moment, $M_A = M_B$, and an axial force F_x applied at both ends.

Given that the axial force does not contribute to beam section rotation, it is excluded from the calculation of the section rotation angle.

Under the local coordinates, the section rotation angle is defined as $(\partial u_x / \partial y)_{y=0}$, where u_x and y are the horizontal displacement component and vertical coordinate, respectively. y=0 corresponds to the location of the middle layer.

2.1.2.1. Bending moment, M_B

For a pure bending beam, the rotation angle at the section center of the beam's end (at x=L) is given by Timoshenko & Goodier[10]:

$$\alpha_3 = -\frac{M_B L}{EI} \quad \text{(XIV)}$$

This result matched the end slope of the beam axis in beam theory,[14] as the assumption that the beam sections remain planar held true.

2.1.2.2. Uniform distributed load, p

The rotation angle at section B under uniformly distributed load can be calculated by Equation XV[10,11]:

$$\alpha_4 = p\, K_2/E \quad \text{(XV)}$$

where:

$$K_2 = -\frac{L^3}{3I} + \frac{L}{4I}\left(\frac{1}{5} + \frac{\mu}{2}\right)(b-a)^2 \quad \text{(XVI)}$$

Here, *I* is the second moment of the area.

The first term in Equation XVI is the result of the beam theory,[14] while the second term represents the shear effect on deformation.

2.2. Bending moment at section B

As the common section, the rotation angle from both sides of section B should be identical, where $\alpha_1+\alpha_2=\alpha_3+\alpha_4$ his condition requires that the bending moment M_B satisfies the following expression:

$$M_B = pC_1/C_2 \quad \text{(XVII)}$$

where:

$$C_1 = \frac{2\pi ab}{N_1}\left[2ab\ln\left(\frac{b}{a}\right) - (b^2-a^2)\right] + K_1 + K_2 \quad \text{(XVIII)}$$

$$C_2 = \frac{4\pi\left(b^2-a^2\right)}{N_1} + \frac{L}{I} \quad \text{(XIX)}$$

Once the bending moment M_B is determined, the forces and moments at any section can be calculated. For example, the bending moments in sections D and C are:

$$M_D = p(C_1/C_2 + L^2/2) \quad \text{(XX)}$$

$$M_C = p(C_1/C_2 - L(a+b)/2) \quad \text{(XXI)}$$

Under the internal pressure, a ring expands evenly. However, an obround shell tends to become more rounded, that is, section D moves outward while section C moves inward.

If M_D is considered positive, then M_C should be negative. The hoop tensile stress occurs on the outer surface of the positive bending moment section and on the inner surface of the negative bending moment section. Due to the continuity of the geometry and load boundaries of the analysis model, it is expected that from section C to section D, the bending moment will smoothly transition from M_C to M_D. M_C and M_D should be the maximum negative and positive bending moments in the shell, respectively. Consequently, the maximum hoop stresses should occur on the inner surface of section C or the outer surface of section D. C_i and D_o are used to represent those two positions (Figure 1).

2.3. Stress

In axisymmetric or plane stress issues, there are two normal stresses (tangential or axial and radial or transversal) and one shear stress. Due to the linear system (geometry and material), the superimposition principle is valid to obtain full stress.

2.3.1. Curved segment BC

Under the local polar coordinate system, stress components are described as follows:[10]

$$\sigma_\theta = \frac{pa^2}{b^2-a^2}\left(1+\frac{b^2}{r^2}\right) + p\frac{L}{N_2}\left[\frac{a^2b^2}{r^3} + \frac{\left(a^2+b^2\right)}{r} - 3r\right]\cos\theta + \frac{4M_{B2}}{N_1}\left(b^2 - a^2 + b^2\ln\frac{r}{b} + a^2\ln\frac{a}{r} - \frac{a^2b^2}{r^2}\ln\frac{b}{a}\right) \quad \text{(XXII)}$$

$$\sigma_r = \frac{pa^2}{b^2-a^2}\left(1-\frac{b^2}{r^2}\right) - p\frac{L}{N_2}\left[\frac{a^2b^2}{r^3} - \frac{\left(a^2+b^2\right)}{r} + r\right]\cos\theta + \frac{4M_{B2}}{N_1}\left(b^2\ln\frac{r}{b} + a^2\ln\frac{a}{r} + \frac{a^2b^2}{r^2}\ln\frac{b}{a}\right) \quad \text{(XXIII)}$$

$$\tau_{r\theta} = \frac{pL}{N_2}\left[\frac{a^2b^2}{r^3} - \frac{\left(a^2+b^2\right)}{r} + r\right]\sin\theta \quad \text{(XXIV)}$$

The first terms in Equations XXII and XXIII are the result of an internal pressure ring or Lame's solution. The remaining terms (in all three equations) are the result of introducing the straight segment AB.

When the length of the straight segment approaches zero (L=0), the obround becomes a ring. In this case, the bending moment M_B should be M_{B1} or M_{B2}=0. The stress expressions of the obround shell, Equations XXII to

XXIV, reduce to Lame's solution. These equations can be considered as extensions of the Lame's solution.

2.3.2. Straight segment AB

In the local rectangular coordinates, the stress components are expressed as Timoshenko & Goodier,[10] Xu[11]:

$$\sigma_x = \frac{M_B}{I}y + p\frac{a}{t} + \frac{6p}{t^3}\left(L^2 - x^2\right)y + \frac{py}{5t^3}(20y^2 - 3t^2) \quad \text{(XXV)}$$

$$\sigma_y = -p\left[2(\frac{y}{t})^3 - \frac{3y}{2t} + \frac{1}{2}\right] \quad \text{(XXVI)}$$

$$\tau_{xy} = -p\left[\frac{3}{2} - 6(\frac{y}{t})^2\right]\frac{x}{t} \quad \text{(XXVII)}$$

where t=(b−a) is the wall thickness of the obround shell.

Here, σ_x is significantly larger than σ_y and τ_{xy}.

The first three terms in Equation XXV match the results of the beam theory.[14] The linear stress distribution of beam theory is the consequence of the assumption that "plane sections remain plane."

The last term of Equation XXV is a nonlinear correction term. Its maximum value is 0.2*p* at the edge of the section, y=±t/2. This term is identical for any section within the straight segment. As the value of this term is relatively small compared to the sum of the other terms, the non-linear behavior poses minimal effect on the stress distribution.

When the length of the straight segment shrinks to zero, sections B and D coincide. In contrast to Equation XXII, the normal stress distribution of Equation XXV differs considerably from Lame's solution, indicating that the stress distribution in section B may not be accurately represented.

2.4. Displacements

Once stress is determined, the corresponding displacements can be derived according to the elastic theory method.[10,11]

As the displacement difference between the inner and outer surfaces is negligible, this paper defines the displacements of the obround shell as those at the middle layer of the shell, that is, the layer of $r=r_0$ within the curved segment, or y=0 within the straight segment. As a result, the displacements become functions of θ or *x* only.

While the derivation process of displacements is relatively complicated, the derived displacement expressions are presented below.

2.4.1. Curved segment BC

In polar coordinates, u_r and v_t are used to represent the radial and tangential displacement components. Under internal pressure, the center of section C undergoes a significant displacement in the global X direction. δ_0 is used to represent this displacement.

In Section 2.1.1, δ_0 was considered as the body motion of the curved segment and thus neglected, as it did not affect the load or stress results.

However, δ_0 is the main part of the horizontal displacement at section C, where it maintains the continuity of displacement at section B.

u_r and v_t can be calculated by Equations XXVIII and XXIX:

$$u_r = \frac{a^2p}{(b^2-a^2)E}\left[\frac{(1+\mu)b^2}{r_0} + (1-\mu)r_0\right] - K_3(1-\cos\theta) + \frac{2pL}{EN_2}\left(b^2 + a^2\right)\theta\sin\theta + \delta_0\cos\theta \quad \text{(XXVIII)}$$

$$v_t = \frac{8M_{B2}}{EN_1}\left(b^2 - a^2\right)r_0,\ -\left(K_3 + K_4 + \delta_0\right)\sin\theta + \frac{2pL}{EN_2}\left(b^2 + a^2\right)\theta\cos\theta \quad \text{(XXIX)}$$

$$K_3 = \frac{4M_{B2}}{EN_1}\left\{\begin{array}{l}\left(b^2 - a^2\right)\left[1 - (1-\mu)\ln r_0\right]r_0 + \dfrac{(1+\mu)a^2b^2}{r_0} \\ \ln\left(\dfrac{b}{a}\right) + (1-\mu)\left(b^2\ln b - a^2\ln a\right)r_0\end{array}\right\} \quad \text{(XXX)}$$

$$K_4 = \frac{pL}{EN_2}\left[(3-\mu)r_0^2 + (1+\mu)\left(a^2 + b^2 - \frac{a^2b^2}{r_0^2}\right)\right] \quad \text{(XXXI)}$$

The determination of δ_0 needs to consider the consistent displacement of the straight segment shell at section B in *x* direction.

2.4.2. Straight segment AB

The displacement components in the local *x* and *y* directions are denoted as u_x and v_y. They are calculated using Equations XXXII and XXXIII:

$$u_x = \frac{p}{E}(\frac{\mu}{2} + \frac{a}{t})x \quad \text{(XXXII)}$$

$$v_y = \frac{p}{20Et^3}\left[60L^2 - 10\left(L^2 + x^2\right) + (24 + 15\mu)t^2\right]\left(L^2 - x^2\right) + \frac{6M_B}{Et^3}\left(L^2 - x^2\right) + v_0 \quad \text{(XXXIII)}$$

where, v_0 is the displacement of section B in *y* direction from the curved segment, with the value of $(u_p)_{\theta=\pi/2}$.

$$v_0 = \frac{a^2 p}{(b^2 - a^2)E}\left[\frac{(1+\mu)b^2}{r_0} + (1-¼)r_0\right]$$
$$-K_3 + \frac{\pi pL}{EN_2}\left(a^2 + b^2\right) \quad \text{(XXXIV)}$$

At section B, the positive directions of v_t and u_x are opposite. However, the displacement of section B should be identical from both sides of the section, that is, $(u_x)_{x=L}=-(v_t)_{\theta=\pi/2}$. Therefore, the value of δ_0 can be determined as:

$$\delta_0 = \frac{4\pi M_{B2}}{EN_1}\left(b^2 - a^2\right)r_0 - \left(K_3 + K_4\right) + \frac{pL}{E}\left(\frac{\mu}{2} + \frac{a}{t}\right) \quad \text{(XXXV)}$$

Meanwhile, the maximum displacements of an obround shell in global X and Y directions occur on the symmetrical planes. They are defined as $\delta_D=(v_y)_{x=0}$ and $\delta_C=(u_r)_{\theta=0}$. These are given by:

$$\delta_D = \frac{M_B L^2}{2EI} + \frac{pL^2}{240EI}\left[50L^2 + (24+15\mu)t^2\right] + v_0 \quad \text{(XXXVI)}$$

$$\delta_C = \frac{a^2 p}{\left(b^2 - a^2\right)E}\left[\frac{(1+\mu)b^2}{r_0} + (1-\mu)r_0\right] + \delta_0 \quad \text{(XXXVII)}$$

The term v_0 represents the vertical displacement in section B. It is the result of internal pressure and the corresponding end loads of the curved segment.

Both δ_C and δ_0 describe horizontal displacements at the center of section C. δ_C is the real displacement, whereas δ_0 is the virtual one used to maintain the displacement continuity at the junction.

The first term of Equation XXXVII (from the pressure ring) is much smaller than δ_0. It can be considered as $\delta_C \approx \delta_0$.

For plane strain issue, E and μ in Section 2.4 should be replaced by $\frac{E}{1-\mu^2}$ and $\frac{\mu}{1-\mu}$, respectively.

3. Discussion

The stress distribution expressions in Equations XXII – XXVII resulted from superposing the stress distributions of the existing closed-form solutions in elasticity theory. An additional deformation condition introduced in the analysis was that, at the junction of the curved and straight segments, the displacement and rotation angle at the section center are continuous. Based on this continuity condition, the bending moment at the junction was obtained. With this value, the bending moments at any other section can then be calculated. The displacement components of the middle layer of the shell are derived from stress distributions. The maximum displacements in the global X and Y directions, δ_c and δ_D, were also obtained.

For cylindrical shells, the maximum hoop stress is one of the most critical factors in the design process. Similar to a cylinder shell, the hoop stress of an obround shell is defined as the tangential stress of the curved segment σ_θ and axial stress of straight segment σ_x. This implies that the direction of hoop stress is parallel to the edge of the obround section.

As there are no geometric and load discontinuities, the stress distribution on the section can be assumed to vary smoothly along θ (curved segment) or *x* (straight segment). The section with the greatest bending moment should be the section with the greatest hoop stress. Therefore, the maximum stress should occur at sections C or D or locations C_i or D_o. For design purposes, only the stresses at C_i and D_o need to be concerned. These sections are located far from junction or section B; hence, the calculated stresses at C_i and D_o are expected to be accurate.

The ASME Code considers hoop stress in obround shells to consist of bending stress and membrane stress. The stresses at the inner and outer surfaces of sections B, C, and D need to be calculated to compare with allowable limits.[1,2] From the above analysis, the stress at section B was lower than at sections C and D. Therefore, stress at section B can be safely disregarded.

Due to tensile membrane stress, the maximum stress always occurs at the tensile side. Thus, only the stresses at C_i and D_o should be concerned.

In addition, the shear stress in an obround shell is relatively small and is therefore ignored in the following discussion.

The expressions of displacement, Equations XXVIII – XXXVII, are discussed and compared with FEA results.

3.1. Stress distributions

An example of FEA was analyzed. In this example, a thick-walled obround shell was chosen to exaggerate possible stress errors and nonlinear stress behavior.

In this paper, the two-dimensional element of plane183 of Ansys was used to perform FEA. A square element shape was used. The mesh size was 1/20 of the wall thickness. The parameters of the obround shell used in FEA were a=300 mm, b=600 mm, L=380 mm, and p=8 MPa.

Material properties used were E=210 GPa and μ=0.3.

The hoop stress and radial stress are defined as σ_θ and σ_r for the curved segment BC, and σ_x and σ_y for the straight segment AB.

Figures 5 and 6 are the hoop and radial stress distribution curves at section C, θ=0, and at section D, x=0. The linear curves in Figure 5 are the sum of membrane and bending

stresses based on the tangential forces (Equations I and II) and bending moments (Equations XX and XXI) of sections.

The hoop stress distribution was nonlinear in section C and approximately linear in section D.

As there are no geometry and load boundary condition discontinuities from segments C to D, hoop stress distribution on the section was expected to change smoothly. When the section moved from section C to section D, the hoop stress distribution on the section would turn counterclockwise from the curve $(\sigma_\theta)_{\theta=0}$ in Figure 5 to curve $(\sigma_x)_{x=0}$, and from significant nonlinear to linear. The tensile hoop stress should move from C_i to D_o.

The ASME Code uses membrane plus bending stress as the design stress. The curves in Figure 5 show that using membrane plus bending stress as hoop stress may lead to an underestimation. In this case, the hoop stress was 27% higher than the membrane plus bending stress.

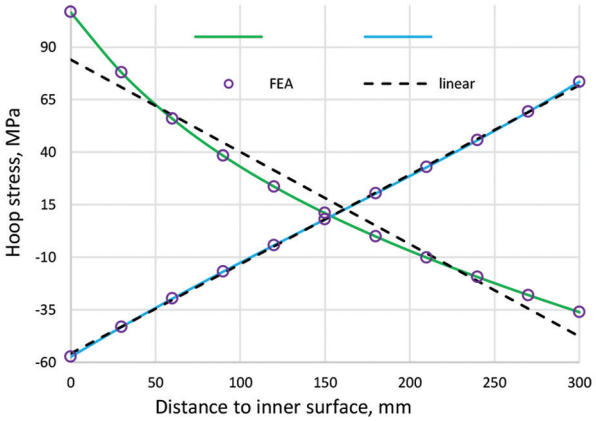

Figure 5. Hoop stress, $(\sigma_\theta)_{\theta=0}$ (green line) and $(\sigma_x)_{x=0}$ (blue line), sec. C
Abbreviation: FEA: Finite element analysis.

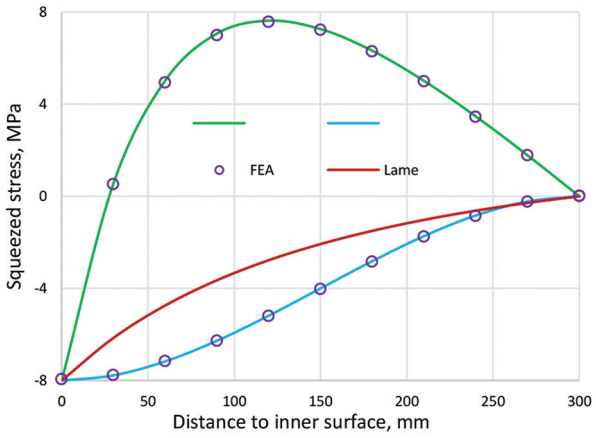

Figure 6. Radial stress, $(\sigma_r)_{\theta=0}$ (green line) and $(\sigma_y)_{x=0}$ (blue line), sec. C
Abbreviation: FEA: Finite element analysis.

Radial stress was in tension through most of the thickness of section C but in compression across the entire thickness of section D (Figure 6). Radial stress in the shell was much smaller than hoop stress.

As sections C and D were located far from section B, the proposed expressions of stress distribution were expected to be accurate.

Figures 7 and 8 show the hoop and radial stress distributions at section B across the thickness from both sides of section B, $(\sigma_\theta)_{\theta=\pi/2}$ and $(\sigma_x)_{x=L}$. The averaged curve demonstrated in Figure 7 was obtained by taking the average of the results from Equations XXII and XXV.

At the junction, the calculated stresses from the curved beam and straight beam were inconsistent because only consistency of displacement and rotation angle at the

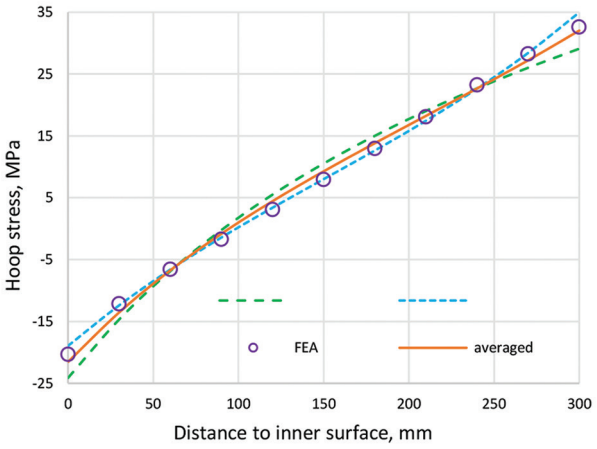

Figure 7. Hoop stress, $(\sigma^\theta)_{\theta=\pi/2}$ (green dashed line) and $(\sigma_x)_{x=L}$ (blue dashed line) sec. B

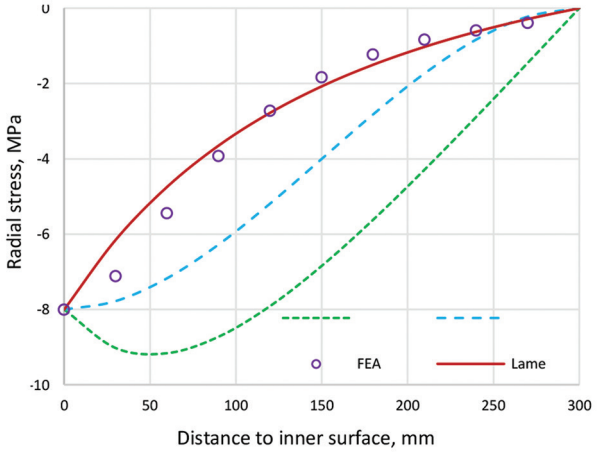

Figure 8. Radial stress, $(\sigma_r)_{\theta=\pi/2}$ (green dashed line) and $(\sigma_y)_{x=L}$ (blue dashed line), sec. B
Abbreviation: v_y: Displacement of straight segment.

center of this section was required in the analysis. The difference between the two was small, and their average provides a good approximation.

The hoop stress distribution of Section B was similar to that of Section D, that is, the tension stress occurred at the outer surface. This suggests that the section where the hoop tensile stress shifted from the inner surface to the outer surface is located between section C and section B.

In section B, the radial stress obtained using either Equation XXIII or XXVI was inaccurate. Lame's solution provided a better result, even though this section is not a symmetry plane (Figure 8).

The first and last terms in Equations XXII and XXIII are independent functions of θ. They are axisymmetric terms and apply uniformly to all sections within the curved segment. The curves of $(\sigma_\theta)_{\theta=\pi/2}$ and $(\sigma_r)_{\theta=\pi/2}$ in Figures 7 and 8 represent these functions.

For design purposes, the maximum hoop stress is the most important stress component. For pressurized obround shells, the maximum hoop stress occurs at either C_i or D_o. The FEA results confirm that expressions of stress developed in this paper are valid and accurate, even for cases with very thick walls. The error resulting from neglecting the continuity of the most mechanical variables at the junction is very small and can be considered negligible.

3.2. Displacements

An FEA example was carried out to verify the shell displacements. The parameters of the obround shell were the same as those used in Section 3.1, except for b=330 mm, L=600 mm, and p=0.1 MPa.

The radial and tangential displacement components within the curve segment are shown in Figure 9.

The radial displacement curve v_t showed that near the middle of the curved segment (θ≈48°), the radial displacement u_r was zero. The deformation of the curved segment seemed to result from the rotation around the point θ≈48°. The portion of the shell before this point moved toward the center of the obround, while the portion after this point moved in the opposite direction. To keep the plane of symmetry from rotation, the opposite rotation was applied to section C. The value of u_r at $\theta=\frac{\pi}{2}$ was greater than that at θ=0, that is, $v_0=(u_r)_{\theta=\frac{\pi}{2}}$ was $>\delta_C=(u_r)_{\theta=0}$. The curve of u_r was nonlinear before this point and linear after the point.

Figure 10 exhibits the deflection of a straight shell v_y from section B (x=600 mm) to section D (x=0 mm).

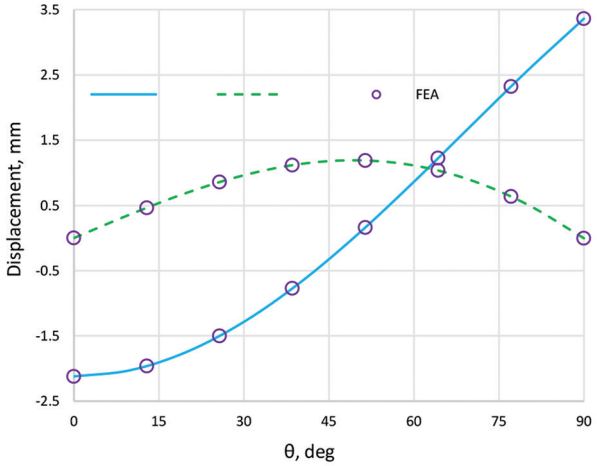

Figure 9. Displacement of curved segment, u_r (blue line) and v_t (green dashed line)
Abbreviation: deg: Degree.

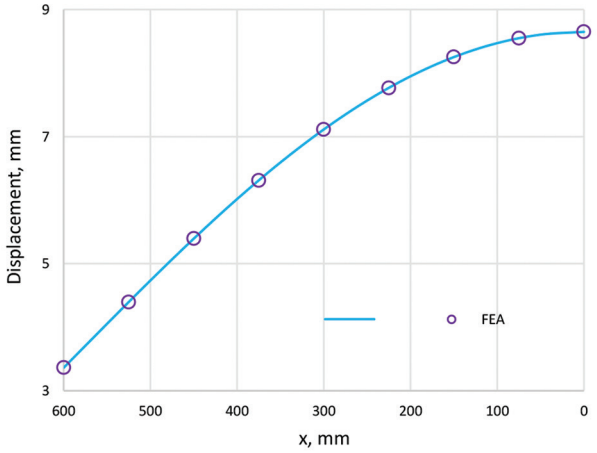

Figure 10. Displacement of straight segment, v_y (blue line)

In the analysis, the straight segment was dealt with as a simple support beam with a rigid body motion v_0 in y direction. v_0 is the minimum deflection of the straight segment. The maximum vertical displacement $\delta_D=(v_y)_{x=0}$ was much greater than the maximum horizontal displacements δ_C In this case, δ_D and δ_C were 8.65 mm and −2.12 mm, respectively. The directions of δ_C and δ_D were in the negative X direction and positive Y direction, respectively.

Table 1 summarizes the displacement results for different geometries under a pressure of 1 MPa. All displacements listed in Table 1 were calculated under the plane stress state. For the plane strain issue, E and μ in the related expressions (Equations XXVIII – XXXVII) should be replaced with $\frac{E}{1-\mu^2}$ and $\frac{\mu}{1-\mu}$, respectively.

Table 1. Displacement results, 10^{-3} mm

a	b	L	δ_C, 10^{-4}mm		δ_D, 10^{-4} mm		round
mm	mm	mm	Equation XXXVII	FEA	Equation XXXVII	FEA	10^{-3} mm
300	500	380	562	563	1529	1530	69
300	400	380	3388	3389	9137	9137	126
300	330	380	98933	98933	277333	277333	387
300	330	600	212069	212069	864805	864805	524

Abbreviation: FEA: Finite element analysis

Poisson's ratio μ had little effect on displacement. From an engineering perspective, this impact is negligible. However, due to the reciprocal relationship between displacement and Young's modulus E, the displacement decreased by the same percentage as E increased. For the case of μ=0.3, displacements under plane strain state were 10% smaller than those under plane stress issue.

The values in the last column of Table 1 are the maximum displacements for the cylindrical shells with the same inner surface enclosing area, shell thickness, and internal pressure as the corresponding obround shells. The thinner the wall and the longer the flat shell, the greater the displacement ratio between the obround and the cylindrical shells.

4. Conclusion

In this paper, the theoretical analysis of the obround shells under internal pressure was performed, and a closed-form solution was proposed. Although the deformation at the junction of segments was partially satisfied, the proposed combined solution accurately described the stress and displacement distributions of obround shells. Considering the uniqueness of the elastic solution, the proposed solution can be considered the closed-form solution for pressurized obround shells.

Using the proposed solution, the theoretical analysis can be easily performed without the complicated and time-consuming pre- and post-processing typically required in numerical analysis.

Based on the above discussion, the following conclusions are drawn:

(i) Under the framework of elastic theory, a closed-form solution for the pressurized obround shells is developed. This is a combination of the existing solutions. It can be considered an extension of Lame's solution.

(ii) Stresses and displacements are accurately determined at any location.

(iii) The maximum stress of an obround shell always appears at the edges of one of the symmetrical sections due to the maximum bending moments.

(iv) The maximum displacement occurs in symmetrical planes. They increase significantly compared to those of cylindrical shells.

(v) With the closed-form solution, a parameter study of an obround shell becomes possible.

(vi) The proposed method offers a powerful approach for the design of obround flanges, pipes, vessels, and other engineering applications, serving as an alternative to empirical or numerical analyses.

(vii) The proposed method can serve as a useful tool for establishing and developing design methodologies and addressing the gaps in current design codes.

Nomenclature

Symbol (s)	Definition
a, b	Inside and outside radius of curved segment of obround
L	Half-length of straight segment of obround
X, Y	Global coordinates
r, θ	Local polar coordinates
r_0	Radius of middle layer of curved segment ($r_0 = \frac{b+a}{2}$)
x, y	Local rectangular coordinates
t	Thickness of shell (t=b – a)
I	Second moment of area
p	Internal pressure
F_x	Axial forces in flat shell
F_y	Tangential force at the fixed end of curved segment
F_{Ay}, F_{By}	Transversal forces at sections A and B (F_{Ay}=F_{By})
M_i	Bending moment at section i (i=A, B, C, D)
M_{B1}	Bending moment in pressurized ring
M_{B2}	Bending moment component at section B used to calculate rotation angle (M_{B2}=M_B–M_{B1})
α_i	Rotation angle (i=1, 2, 3, …)
N_1, N_2	Size-related parameters
C_1, C_2	Parameters
Ki	Parameters
σ_θ, σ_r, $\tau_{r\theta}$	Stress components in polar coordinates
σ_x, σ_y, τ_{xy}	Stress components in rectangular coordinates
C_i, D_o	Maximum hoop stress location
u_r, v_t	Displacement components in polar coordinates
u_x, v_y	Displacement components in rectangular coordinates
δ_C, δ_D	Maximum displacement in global X and Y directions
δ_0	Horizontal displacement to maintain the displacement continuity at junction
v_0	Vertical displacement at the center of section B
E, μ	Young's modulus, Poisson's ratio of material

Acknowledgments

None.

Funding

None.

Conflict of interest

The author declares no conflicts of interest. Propak Systems Ltd. had no role in the design, analysis, or interpretation of the work.

Author contributions

This is a single-authored article.

Ethics approval and consent to participate

Not applicable.

Consent for publication

Not applicable.

Availability of data

All data are included in the paper. If readers need more detail, extra information can be provided.

Further disclosure

The main idea of this paper was presented at the Pressure Vessels and Piping Conference (PVP) 2023, held at the Westin Peachtree Plaza, Atlanta, Georgia, United States, from July 16 to July 21, 2023. The paper is included in the PVP-2023 proceedings (ASME 2023 Pressure Vessels and Piping Conference Proceedings, Volume 2: Computer Technology and Bolted Joints; Design and Analysis).

References

1. ASME. *Boiler and Pressure Vessel Code, Section VIII Div. 1. Rules for Construction of Pressure Vessels*. New York: ASME; 2019.
2. ASME. Boiler and Pressure Vessel Code, Section VIII Div. 2. Alternative Rules New York: ASME; 2019.
3. Blach AE. *Non Circular Pressure Vessel Flanges: New Design Methods*. Germany: Fluid Sealing, Springer-Science and Business Media; 1992. p. 247-265.
4. Zheng QS. *Analysis of a Shell of Elliptical Cross-Section under Internal Pressure and Body Force*. [PhD Dissertation]. Lubbock, TX: Mechanical Engineering Texas Tech University; 1997.
5. Singh KP. An efficient design method for obround pressure vessels and their end closures. *Int J Press Vessels Piping*. 1977;5(4):309-320.

   doi: 10.1016/0308-0161(77)90010-2
6. Shah YP, Pradhan MN. Design of obround flange for pressure vessel application by analytical method and FEA to comply with ASME code. *Int J Adv Res Innov Ideas Educ*. 2013;1(2):211-221.
7. Utagikar MM, Naik SB. Finite element analysis of obround pressure vessels. *Int J Mod Eng Res*. 2013;3(5):2719-2727.
8. Utagikar MM, Naik SB. Finite element analysis of elliptical pressure vessels. *Am J Eng Res*. 2013;2(12):343-349.
9. Pany C. Investigation of circular, elliptical and obround shaped vessels by finite element method (FEM) analysis under internal pressure loading. *J Sci Technol Eng Res*. 2022;3(1):24-31.

   doi: 10.53525/jster.1079858
10. Timoshenko S, Goodier JN. *Theory of Elasticity*. New York: McGraw-Hill Book Company Inc.; 1951.
11. Xu Z. *Theory of Elasticity*. Beijin: Higher Education Press; 1978.
12. Jin Y. A new design method for obround shells. J Pressure Vessel Technol. 2024;146(3):031302.

    doi: 10.1115/1.4065175
13. Jin Y. *Research on Stress in Obround and Out-of-roundness Shells*. [ASME Paper No. PVE2024-121933]; 2024.
14. Timoshenko S. *Strength of Materials*. D. New York: Van Nostrand Company Inc; 1948.